Contribution of electrical resistivity to the quantification of α and ω_iso phase transformations in Ti-15Mo and Ti-10Mo titanium alloys

B. Denand, Y. Le Bouar, F. Lebel, B. Appolaire

Contribution of electrical resistivity to the quantification of α and ω_{iso} phase transformations in Ti-15Mo and Ti-10Mo titanium alloys

B. Denand[1,2], Y. Le Bouar[3], F. Lebel[1,2], B. Appolaire[1,2]

1 Université de Lorraine, CNRS, IJL, Nancy, France
2 Labex Damas, Université de Lorraine, Nancy, France
3 Université Paris-Saclay, ONERA, CNRS, Laboratoire d'Étude des Microstructures, 92322 Châtillon, France.

The aim of this paper is to evaluate the possibility of quantitatively monitoring the microstructural evolution in titanium alloys during isothermal heat treatment using electrical resistivity measurements. Specifically, the model alloys Ti-10Mo and Ti-15Mo are studied to investigate the transformation sequences β → β + α and β + ω_{ath} → β + ω_{iso}, respectively. To this end, we have combined quantitative in situ resistivity measurements, in situ high energy X-ray diffraction (HEXRD) analysis and microstructural characterisation using scanning electron microscopy (SEM) and transmission electron microscopy (TEM). During annealing at 650 °C of the Ti-10Mo alloy, the microstructure consists of micron-scale α-phase lamellae in the β-matrix, and we show that the increase in resistivity follows that of the α-phase volume fraction. During annealing at 350 °C of the Ti-15Mo alloy, the microstructure is composed of nanometric precipitates of ω phase and we show that the resistivity evolves in a non-monotonic manner, although the fraction of ω always increases. These results cannot be explained by simple models where the description of the microstructure is limited to the phase fraction and suggest the importance of the interfacial contribution to the resistivity in these alloys.

Keywords: Phase transformations, electrical resistivity, Ti-Mo, alpha, omega

1. Investigation of precipitates formation by electrical resistivity

Metastable β-Ti alloys are a class of titanium alloys with great potential for use in many industrial sectors, such as aerospace, automotive and biomedical applications, due to their outstanding chemical and mechanical properties [1,2]. Optimisation of these properties requires a deep understanding of the microstructure formation and evolution. It is clear, therefore, that studying the mechanisms and predicting the kinetics are key steps in designing and controlling microstructures with the desired properties. Among the in-situ techniques for characterising microstructure evolution during thermal treatment, electrical resistivity is one of the easiest to use. This technique is known to be sensitive to small microstructural changes, such as the elimination of quenched vacancies [3], dislocation annealing [4], diffusive and displacive phase transformations [5]. All studies using resistivity to investigate phase transformations in titanium-molybdenum alloys have focused on the formation of the ω phase [6-9].

However, although electrical resistivity is sensitive to the microstructure, the quantitative nature of the results is usually limited by the use of phenomenological laws to relate resistivity to microstructural features. In particular, it is generally assumed that the electrical resistivity of a multiphase material follows a simple mixing rule [10], whereas it is known from homogenisation theories [11,12] that the average electrical resistivity should depend on the spatial arrangement of the coexisting phases. It should also be mentioned that the resistivity is also sensitive to the interfaces in the microstructure and this contribution is expected to be important when the interface structure/composition is significantly different from that of the neighbouring domains, or in the case of nanoscale heterogeneities (spinodal decomposition, nanometric precipitates...) for which the surface to volume ratio is high. For example, Ho & Collings suggest an interfacial contribution in addition to that of the β and ω phases to explain the high values of the effective resistivity [6].

The aim of this paper is to evaluate the possibility of quantitatively monitoring the microstructural evolution of titanium alloys during isothermal heat treatment using electrical resistivity measurements. The approach consists of measuring resistivity during microstructural evolution and independently characterising the microstructural evolution using in situ high energy X-ray diffraction (HEXRD) and electron microscopy. All these results will allow us to test the relevance of the rule of mixtures, which is often used to analyse resistivity measurements.

Specifically, the model alloys Ti-10Mo and Ti-15Mo are studied to investigate the transformation sequences β → β + α and β + ω_{ath} → β + ω_{iso}, respectively. These two alloys were chosen because they give qualitatively different microstructures. In the Ti10Mo alloy annealed at 650 °C, the microstructure consists of entangled platelets of micrometric size, whereas in the Ti15Mo alloy annealed at 350 °C, nanometric precipitates are expected.

The paper is organised as follows. The next section describes the sample preparation and experimental techniques. The resistivity measurements and

microstructural characterisations for the Ti-10Mo and Ti-15Mo alloys are presented in turn. Finally, the validity of the mixture rule for the resistivity analysis of multiphase materials is discussed.

2. Material and experiments

Two titanium-molybdenum alloys are used in this study. The Ti-10Mo (wt. %) is from Goodfellow and the Ti-15Mo (wt. %) is from Timet company. The mean grain size was determined after β-solution treatment at 900 °C by electron backscatter diffraction (EBSD) maps and the chemical composition was verified by energy dispersive X-ray spectroscopy (EDS) analysis. The β-transus was determined by electrical resistivity and the results are in agreement with the literature [13]. The results are summarised in Table 1.

The thermal treatments consist of a β-solution treatment followed by an isothermal stage at a temperature for which the Ti-Mo diagram calculated in reference [14] predicts the formation of α-phase in the Ti-10Mo and ω phase in the Ti-15Mo. Isothermal treatments are chosen, so that the electrical resistivity of each phase can be assumed to be constant.

In situ electrical resistivity measurements were made using an in-house dilatometer equipped with a lamp furnace. Resistivity was carefully measured using the four-point method [15]. Current switching [16] (or delta method) is used to reduce the influence of thermal gradients and to cancel the thermoelectric voltages

Table 1. Chemical composition and mean β grain size of the Ti-10Mo and Ti-15Mo samples.

	β grains size (µm)	Mo (wt. %)	β transus (°C)
Ti-10Mo	95 +/- 64	10.4 +/- 0.2	790 +/- 2
Ti-15Mo	39 +/- 27	13.8 +/- 0.6	760 +/- 3

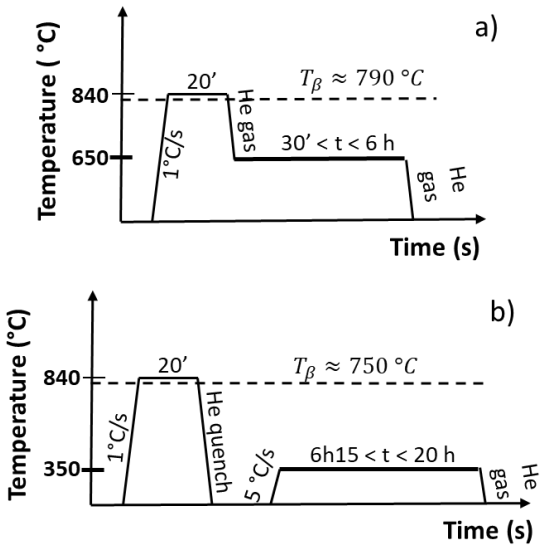

Figure 1. Thermal treatments a) for Ti-10Mo b) for Ti-15Mo.

(mainly Seebeck effect). Frequency noise is minimised by integrating the signal over a power line cycle. In order to obtain the most homogeneous electric field inside the sample [17], a cylindrical shape was chosen with a length between 20 mm and 30 mm for diameters between 4 mm and 6 mm. The development was validated by a good agreement between experiments on pure metals and data from the literature as for pure titanium (Figure 2).

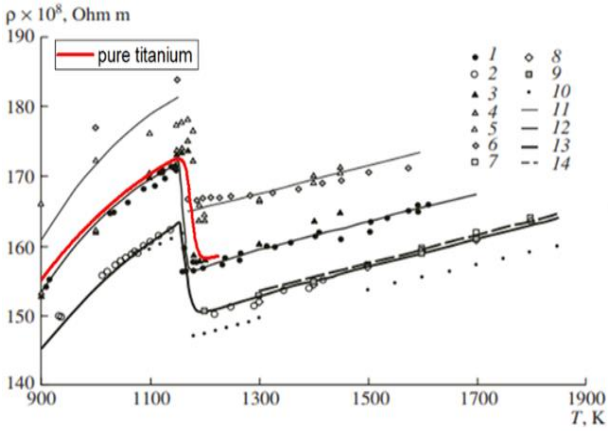

Figure 2. Quantitative comparison of the electrical resistivity of pure titanium during heating: our experiment (red line) versus literature data [18].

Following the approach developed in [19,20], in-situ HEXRD was carried out at DESY at beamline P21.02 using an in-house portable furnace. This device consists of two main components: the rotating sample itself (temperature control) with its environmental chamber, and then the lamp furnace through which the X-ray beam passes (Figure 3). The furnace is designed to perform X-ray diffraction at synchrotron beamlines. This portable furnace has been patented [21].

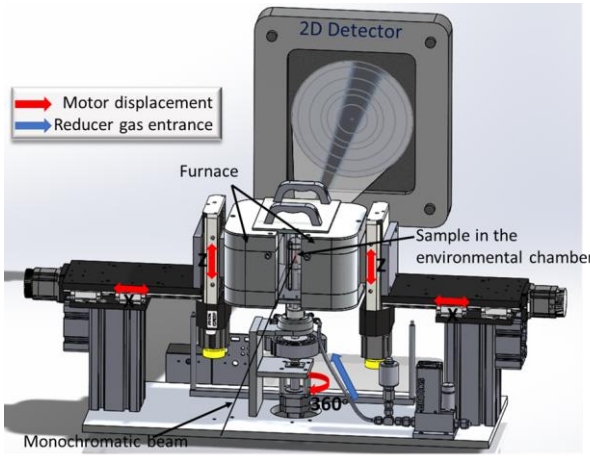

Figure 3. Experimental setup used at DESY at beamline P21.02.

During the experiment, cylindrical samples were irradiated with monochromatic beam of 82.5 keV energy with a beam size of 400 × 400 µm^2. The high energy beam allowed us to analyse a large volume of the sample, which is representative of the bulk and reduces the surface effect. The transmitted signal was collected by a large area 2D detector, which recorded the entire Debye-Scherrer rings with a maximum 2θ angle of 10° every 1 s, corresponding to a complete rotation of the sample along its axis.

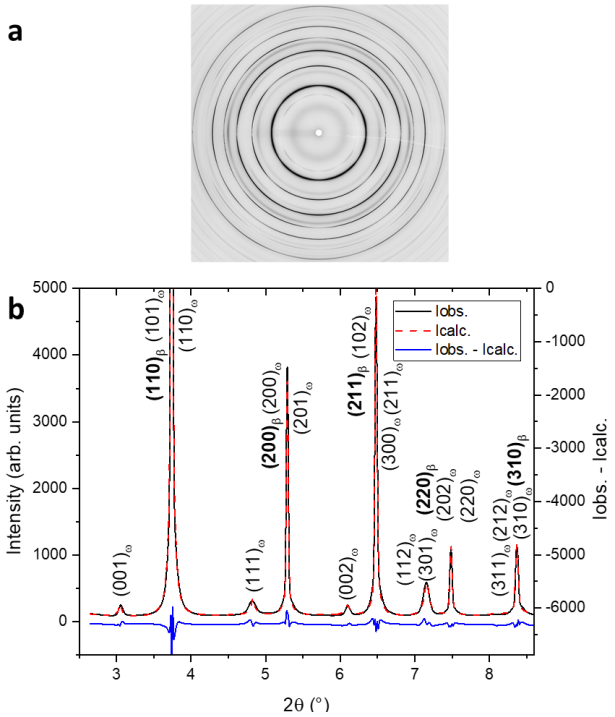

Figure 4. End of ageing at 350 °C of Ti15Mo a) Continuous Debye-Scherrer rings b) Circular integrated and Rietveld analysis (the most intense peaks, I = 30000, are cropped to give a better view of the ω phase peaks).

Therefore, a large number of β grains are irradiated to obtain continuous Debye-Scherrer rings, corresponding to many crystallographic planes, as shown in Figure 4. Integration of the intensities was performed all around the rings. Rietveld analysis was then performed using Fullprof software [22] to extract phase fractions and average cell parameters. A representative result illustrating the quality of the fit is shown in Figure 4b.

Microstructural observations and chemical composition measurements were performed out on a Zeiss Gemini SEM 500 equipped with an EDS detector. Nanoscale observations and chemical analyses were carried out using a JEM-ARM200F ACCELARM transmission electron microscope. Thin samples for TEM characterisation were prepared using a FEI Helios NanoLab 600i DualBeam equipped with the Focused Ion Beam (FIB) technology.

3. Results

3.1 Ti-10Mo: $\beta \rightarrow \alpha + \beta$ transformation

Electrical resistivity and HEXRD measurements of Ti-10Mo samples were carried out at 650 °C. Figure 5 shows the time evolution of the relative electrical resistivity $\Delta\rho = \rho - \rho_0$, where ρ_0 is the resistivity at the start of the isothermal annealing stage.

We observe a continuous increase in resistivity with a continuously decreasing slope. A similar behaviour has also been reported during the α-precipitation in other β-metastable titanium alloys [23]. The volume fraction of α precipitates f_α obtained by HEXRD during the isothermal stage is also shown in Figure 5. As expected, f_α increases rapidly during the growth stage (annealing time less than about 2 h) and then asymptotically reaches a plateau in the coarsening stage. The resistivity of the Ti-10Mo sample and the volume fraction of α-precipitates exhibit very similar evolutions during the isothermal annealing stage. This point will be further discussed in section 4.

The microstructure evolution is shown in Figure 6: it is typical of the α precipitation at high temperatures with an increasing number of long parallel α plates that thicken with time.

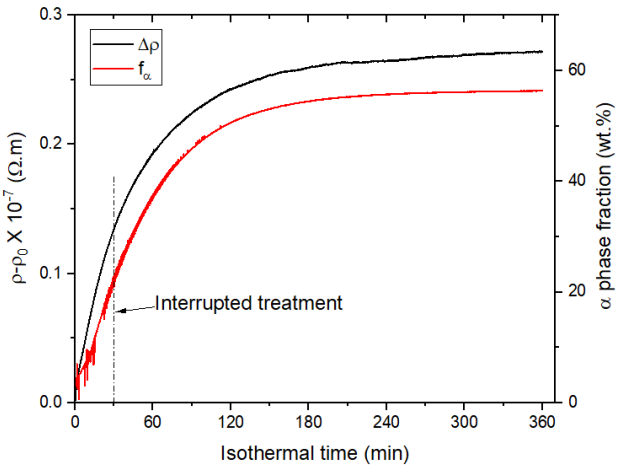

Figure 5. Time evolution of the electrical resistivity (black curve) and the fraction of α (red curve) at 650 °C in Ti-10Mo. The vertical line indicates the annealing time of the microstructure shown in Figure 66a.

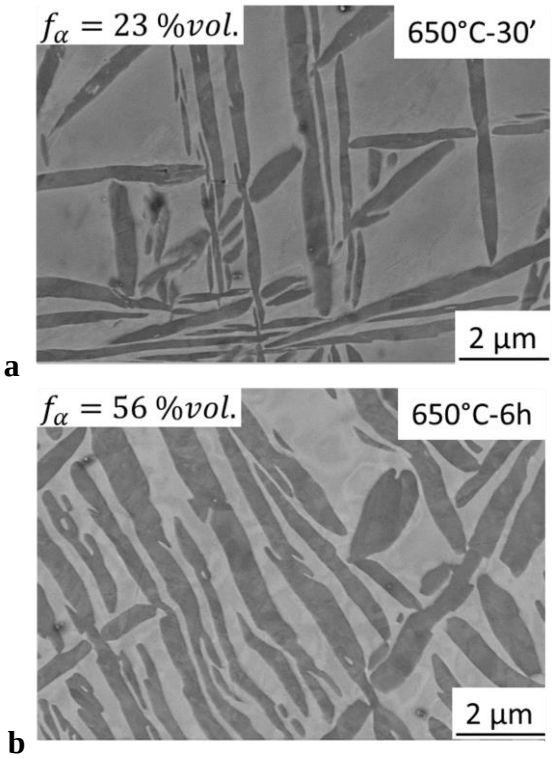

Figure 6. SEM micrographs of the microstructure in the Ti-10Mo alloy annealed at 650 °C for (a) 30 min.; (b) 6h.

3.2 *Ti-15Mo: $\beta + \omega_{ath} \rightarrow \beta + \omega_{iso}$ transformation*

The same procedure was applied to Ti-15Mo at 350°C, using TEM to characterise the microstructural evolution. The time evolution of the relative electrical resistivity is shown in Figure 7a. Contrary to the previous section, it is not monotonous. $\Delta\rho$ increases steeply for about 1 h. It then decreases slightly (over about 1 µΩ × cm) with a decreasing slope and seems to tend towards an asymptotic value that would be reached at a duration much greater than 10 h.

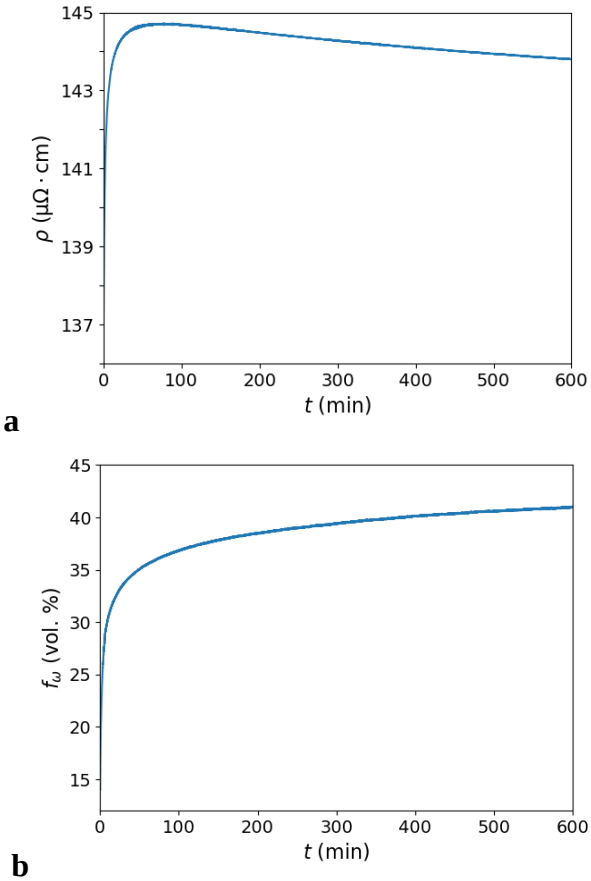

Figure 7. Ti-15Mo during ageing at 350 °C: evolutions of (a) the electrical resistivity; and (b) the volume fraction of ω.

As shown in Figure 7b, the fraction of ω increases monotonically, with an increase of about 20% during the first hour. After 10 hours, the volume fraction has not yet reached an asymptotic value, indicating that the transformation is not complete. Comparing Figure 7a and Figure 7b, the relationship between the evolution of $\Delta\rho$ and f_ω is obviously more complex than for α precipitation.

Dark field TEM observations were carried out on samples quenched for 6 h and 20 h, as shown in Figure 8, to examine their microstructure. A large number of precipitates are observed, in agreement with previous findings in the literature [24,25]. In order to obtain the average precipitate size, numerous clearly visible precipitates were fitted with ellipses. The analysis shows an increase in precipitate size of approximately 0.5 nm between 6 h and 20 h. These measurements are consistent with the XRD measurements.

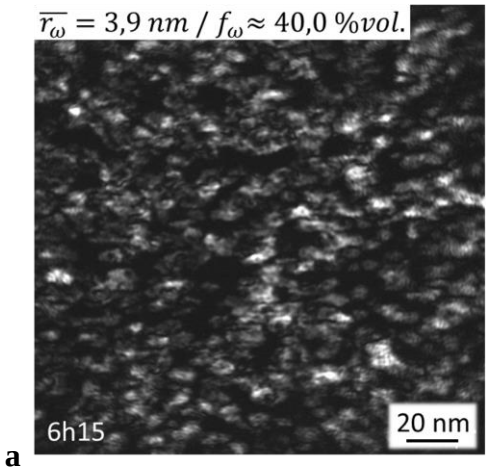

a

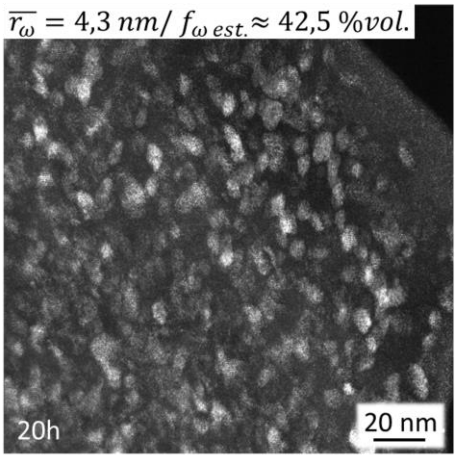

b

Figure 8. TEM images of ω_{iso} precipitating after 6 h and 20 h at 350 °C.

4 Discussion

In order to use resistivity measurements as a quantitative technique to monitor microstructural evolution, it is necessary to relate resistivity to microstructural features.

We first examined the resistivity as a function of the precipitate phase fraction, as is commonly done in the literature [10]. This relationship is shown in Figure 9a for the α phase obtained at 650°C. Although a large part of the curve (f_α > 20%) can be described by a linear fit, a clear non-linear behaviour can be seen at the beginning of the transformation. Looking at the precipitation of the ω phase (Figure 9b), a more linear part can be seen for low volume fraction (f_ω < 30%), but the resistivity curve deviates strongly from the linear behaviour for higher volume fractions. In conclusion, for the two phases transformations considered here, it is clear that the mixing rule is not capable of predicting resistivity over the full volume fraction range.

Instead of using a simple mixing rule, a more physically based approach is to compare our results with theoretical bounds that can be obtained analytically for a two-phase material. Indeed, assuming that the material is macroscopically homogeneous and isotropic, and assuming that the resistivity is isotropic and constant within each phase, it can be shown that the resistivity of the material is bounded by [26]:

$$\rho_L = \frac{\rho_1}{1 + \frac{f_2}{\frac{\rho_2}{\rho_1 - \rho_2} + \frac{f_1}{3}}}$$

$$\rho_U = \frac{\rho_2}{1 + \frac{f_1}{\frac{\rho_1}{\rho_2 - \rho_1} + \frac{f_2}{3}}}$$

where ρ_i and f_i are respectively the resistivity and volume fraction of phase i $\in\{1,2\}$.

Using the linear part of the resistivity curves to estimate the resistivity of each phase, the Hashin-Shtrikman bounds can be determined (Figure 9). It appears that the two bounds are very close to each other, a consequence of the small difference in resistivity between the two phases. This also implies that the values of the bounds are close to the resistivity predicted by the mixing rule.

Figure 9b shows that for volume fractions below 30%, the resistivity during ω precipitation is not too far from the values of the bounds, but the curvatures have different signs. In addition, for volume fractions above 30%, the measured resistivity deviates strongly from the bounds. This implies that the assumptions under which the bounds are obtained are not fulfilled during the precipitation of the ω phase. It may be that the phases are not homogeneous due to compositional gradients. Another explanation could be the importance of a specific resistivity of the interface. Indeed, due to the nanometric size of the ω precipitates, the material necessarily contains a high density of interfaces. This explanation is consistent with the decrease in resistivity during the coarsening regime, when the density of interfaces decreases.

Finally, as shown in Figure 9a, the experimental values are not too far from the bounds during the precipitation of the α phase when f_α > 20%. The deviation observed for small volume fractions could also be explained by a contribution of the interfaces to the resistivity. Indeed, the α platelets are thin at the onset of precipitation, implying a high surface to volume ratio.

Further experimental and theoretical investigations are required to clarify these points.

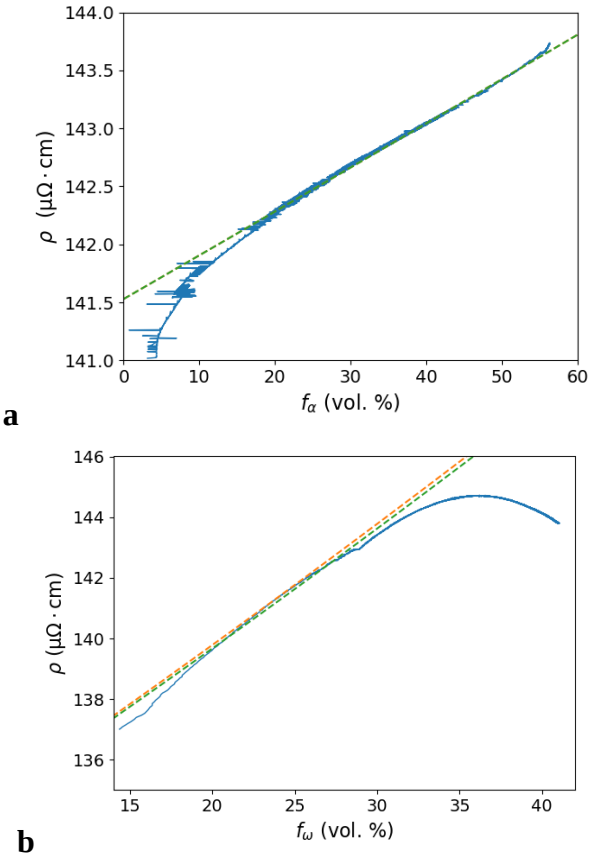

Figure 9. Electrical resistivity (blue) versus volume fraction of precipitates in (a) Ti-10Mo at 650 °C; (b) Ti-15Mo at 350 °C. Hashin-Shtrikman bounds are shown as dashed lines.

5 Conclusion

By combining in situ electrical resistivity measurements and high energy XRD, we have investigated the ability of electrical resistivity measurements to quantify the microstructural evolution in two Ti-Mo alloys undergoing isothermal phase transformations. The evolution of the α phase fraction can be described quite well by a simple mixing rule for volume fractions greater than 20%. This is also consistent with the Hashin-Shtrikman bounds, since the resistivity contrast between α and β is very small. This explains why the determination of kinetic diagrams associated to the β → α transformation using electrical resistivity measurements has been very successful [27].

On the contrary, the evolution of the electrical resistivity during ω_{iso} precipitation is not correctly described by the Hashin-Shtrikman bounds. This discrepancy indicates that contributions not included in the assumptions of the simplest mean-field homogenisation models may play a significant role, so that the quantification of the microstructural evolution in Ti alloys from electrical resistivity measurements requires more sophisticated approaches.

Acknowledgements

This work is part of the ECUME project supported by the French National Research Agency (ANR-18-CE08-0008-02). The authors would like to thank the Deutsches Elektronen-Synchrotron (DESY) for providing beam time at beamline P21.02. We are also grateful to Sylvie Migot and Jaafar Ghanbaja at IJL for their assistance with thin-film preparation and TEM observations. We would also like to thank Guillaume Geandier at IJL for his support at the synchrotron beamline and Alphonse Finel at LEM for his valuable insights into the Hashin-Shtrikam boundaries.

References

1. Lütjering G, Williams JC, Titanium, 2nd ed., Springer, Berlin (2007).
2. Boyer RR, Materials Science and Engineering 213 (1996) 1-2.
3. Wang CG, Seidman DN, Balluffi RW, Physical Review, 169(3) (1968) 553-569
4. Maeta H, Journal of the Physical Society of Japan 24 (1968) 757-762.
5. Rossiter, P. L. The electrical resistivity of metals and alloys 6 (1991). Cambridge university press.
6. Ho J, Collings E, Physical Review B 6 (10) (1972) 3727.
7. Hake R.R., Leslie D. H., Berlincourt T. G., J. Phys. Chem. Solids Pergamon Press, 20 (1961) 314, 177-186
8. Hayman C, Gerberich WW, Metallurgical Transactions A, 16A (1985) 188-195
9. Zhanal P, Harcuba P, Hajek M, Smola B, Strasky J, Smilauerova J, Vesely J, Janecek M, Journal of Materials Science 53 (1) (2018) 837–845
10. Bruneseaux F, Aeby-Gautier E, Appolaire B, Weisbecker P, Mauro A, Materials Science and Engineering A 476 (2008) 60-68.
11. Chang SY, Chen CF, Lin SJ, Kattamis TZ, Acta Materialia, 51 (2003) 6191-6302.
12. Mattissen D, D. Raabe, F. Heringhaus, Acta Materialia, 47(5) (1999) 1627-1634
13. Murray J, Journal of metals 33 (1981) 9.
14. Hu B, Jianga Y, Wang J, Yao B , Min F , Du Y, Calphad 62 (2018) 75-82
15. Laude E, Aeby-Gautier E, Denis S. Proceedings of the 8th World Conference on Titanium, 2330 (1996)
16. Low Level Measurements Handbook - 7th Edition – Tektronix
17. Hajek M, Vesely J, Cieslar M, Materials Science and Engineering A 462 (2007) 339-342
18. Bel'skaya EA, Kulyamina, E, High Temperature 45 6 (2007) 785-796

19. Sharma B, Denand B, Harcuba P, Geandier G, Ameyama K, Dirras G, Aeby-Gautier E, Journal of Alloys and Compounds 860 (2021) 158483

20. Maury N, Denand B, Dehmas M, Archambeau-Mirguet C, Delfosse J, Aeby-Gautier E, Journal of Alloys and Compounds 763 (2018) 446e458

21. Denand B, Dehmas M, Gautier E, Bonnet C, Geandier G, Sarteaux J-P. https://patentscope.wipo.int/search/en/detail.jsf?docId=WO2019081266

22. Rodríguez-Carvajal, J., Commission on Powder Diffraction (IUCr) Newsletter 26 (2001) 12-19.

23. Settefrati A, PhD Thesis, Université de Lorraine (2012).

24. Nejezchlebova J, Janovska M, Sedlak P, Smilauerova J, Strasky J, Janecek M, Seiner H, Journal of Alloys and Compounds 792 (2019) 960-96.

25. Hickman BS, Journal of Materials Science 4 (1969) 554-563.

26. Hashin Z, Shtrikman S, Journal of Applied Physics 33 (1962) 3125-3131.

27. Aeby-Gautier E, Bruneseaux F, Appolaire B, Denis S, JOM 59 (2007) 54-58.